# Theoretical Study of Nuclear Physics with Strangeness at Nankai University

NING Ping-Zhi

(College of Physics Science, Nankai University, Tianjin 300071, China)

**Abstract**　Theoretical study of nuclear physics with strangeness from the nuclear physics group at Nankai university is briefly introduced. Theoretical calculations on hyperon mean free paths in nuclear medium have been done. The other 4 topics in the area of strangeness nuclear physics are the effect of different baryon impurities in nucleus, the heavy flavored baryon hypernuclei, the eta-mesons in nuclear matter and the properties of kaonic nuclei.

**Key words**　nuclear physics, strangeness, hyperon

It's my pleasure to present our work[1—10] from the Nuclear Physics group at Nankai University. I will focus on 5 topics in the area of Strangeness Nuclear Physics. I will go into more details topic by topic.

## 1　Hyperon mean free paths(MFP) in nuclei[1]

Almost nothing has been done in theoretical calculations on hyperon MFP in nuclear medium. It is mainly due to the lack of experimental data on hyperon-nucleon/nucleus interactions. Recently, there are some experimental progresses in this area that improve the conditions for us to study the hyperon MFP in nuclei.

On this topic, we attempt to calculate the hyperon MFP in nuclei within the framework of the relativistic mean-field (RMF) theory. To calculate the hyperon mean free paths in a nucleus, the key point is to construct an energy-dependent hyperon-nucleus optical potential. In our work, we obtain the real scalar and vector hyperon-nucleus potentials from the relativistic mean-field approach. Then following Cooper's work[11],

$$U_{\mathrm{S}}^{IY} = \alpha_{\sigma Y} \cdot U_{\mathrm{S}}^{IN} \quad \text{and} \quad U_{\mathrm{V}}^{IY} = \alpha_{\omega Y} \cdot U_{\mathrm{V}}^{IN} , \qquad (1)$$

we figure out the hyperon-nucleus imaginary potentials from the nucleon-nucleus imaginary potentials. The hyperon optical potentials $U = V + \mathrm{i}W$ can be identified as the Schrodinger equivalent potentials and

$$V = U_{\mathrm{S}}^{RY} + \frac{E}{M_{\mathrm{Y}}} U_{\mathrm{V}}^{RY} + \frac{1}{2M_{\mathrm{Y}}} \big( U_{\mathrm{S}}^{RY2} - U_{\mathrm{V}}^{RY2} +$$
$$\alpha_{\omega Y}^2 U_{\mathrm{V}}^{IN2} - \alpha_{\sigma Y}^2 U_{\mathrm{S}}^{IN2} \big), \qquad (2)$$

$$W = \alpha_{\sigma Y} U_{\mathrm{S}}^{IN} + \alpha_{\omega Y} \frac{E}{M_{\mathrm{Y}}} U_{\mathrm{V}}^{IN} +$$
$$\frac{1}{M_{\mathrm{Y}}} \big( \alpha_{\sigma Y} U_{\mathrm{S}}^{RY} U_{\mathrm{S}}^{IN} - \alpha_{\omega Y} U_{\mathrm{V}}^{RY} U_{\mathrm{V}}^{IN} \big) . \qquad (3)$$

Note that the equation $U = V + \mathrm{i}W$ which are the hyperon optical potentials in the non-relativistic approach, but including the relativistic correction in this term:

$$[(E - MB)2/2MB].$$

Equations (2) and (3) show that the Schrodinger equivalent potentials are energy dependent.

At zero momentum, compared with the usual optical potentials defined in the RMF, the optical potentials equal the scalar potential plus the vector potential ($U_{\mathrm{opt}} = U_S + U_V$). Also in Eqs. (2) and (3),

each Schrodinger equivalent potential has an additional term—that is the third term.

I will talk more later about how much the third term contributes to the Schrodinger equivalent potential. Now we can express the hyperon mean free path as

$$\lambda = \frac{1}{2} \left\{ -M_Y \left( E - M_Y - V + \frac{(E-M_Y)^2}{2M_Y} \right) + \right.$$
$$\left. M_Y \left[ \left( E - M_Y - V + \frac{(E-M_Y)^2}{2M_Y} \right)^2 + W^2 \right]^{\frac{1}{2}} \right\}^{-\frac{1}{2}}. \quad (4)$$

With these determined potentials, we have calculated the hyperon MFP in nuclei. We show that the MFP of $\Lambda$, $\Xi$ in $^{40}$Ca and $^{208}$Pb as a function of $r$ in Fig. 1 and Fig. 2. The solid curves and dotted curves correspond to the hyperon incident energies $T_{lab}=300$MeV and 600MeV, respectively.
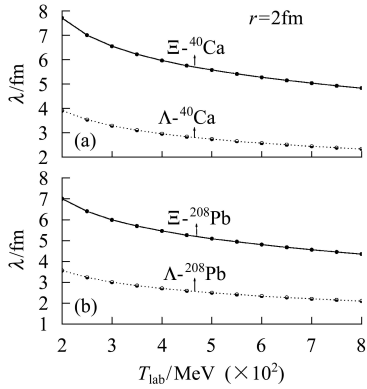


Fig. 1. The $\Lambda$- and $\Xi$-hyperon mean free path as a function of the incident energies, $T_{lab}$, from 200MeV to 800MeV in $^{40}$Ca and $^{208}$Pb at $r=2$fm in (a) and (b), respectively.
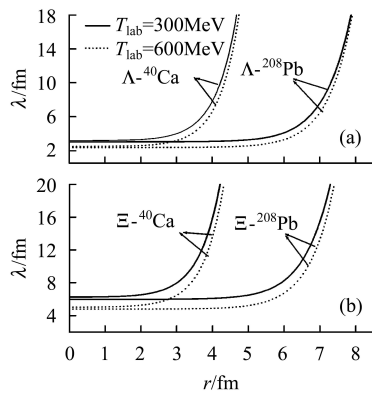


Fig. 2. The hyperon mean free path as a function of the radius in $^{40}$Ca and $^{208}$Pb, with incident energies, $T_{lab}=300$MeV and 600MeV, respectively. Those for the $\Lambda$-hyperon are shown in (a) and those for the $\Xi$-hyperon are shown in (b).

We also find that, in the center of nuclei, the hyperon MFP is about 2—3fm for $\Lambda$, and about 4—8fm for $\Xi^-$, depending on the hyperon incident energy. And the hyperon MFP decreases with the increment of the hyperon incident energy.

This work is only an attempt to calculate the MFP of the hyperon. Owing to the importance of the in-medium properties of the hyperons, more theoretical as well as experimental work on the hyperon mean free path are needed. The study of the temperature dependence of the hyperon MFP is also needed because of the appearance of hyperons in high-energy heavy-ion reactions.

## 2 The effect of different baryon impurities in nucleus[2]

It is well known that the change of bulk properties of nuclei under the presence of strange impurities, like the lambda hyperon, is an interesting subject in hypernuclear physics.

Since a Lambda does not suffer from Pauli blocking in Lambda hypernuclei, it can locate at the center of a nucleus. Consequently, the Lambda attracts the surrounding nucleons and makes the nucleus shrink. Recently, the experiment KEK-PS E419 showed clear evidence for this shrinkage of the $^7$Li Lambda hypernucleus.

How about other strange impurity baryons, such as Sigma-hyperon and Cascade-hyperon or even heavy-flavored baryons? How about the effect of different baryon impurities on the nuclei?

In this work, we demonstrate the above problems and solutions within the framework of the relativistic mean-field model. In the computation of relativistic mean-field, the most important part is to determine the coupling constants. Let's take a closer look at it next.

The coupling constants of hyperons to the vector fields in the native quark-counting model are obtained from these simple equations:

$$g_{\omega\Xi^-} = g_{\omega\Xi^0} = g_{\omega\Xi_c^0} = g_{\omega\Xi_c^+} = \frac{1}{3}g_{\omega N},$$
$$g_{\rho\Xi^-} = g_{\rho\Xi^0} = g_{\rho\Xi_c^0} = g_{\rho\Xi_c^+} = g_{\rho N}, \quad (5)$$
$$g_{\omega\Lambda} = g_{\omega\Lambda_c^+} = g_{\omega\Lambda_b} = \frac{2}{3}g_{\omega N}.$$

The scalar coupling constants for the hyperons are fixed to the potential depth of the corresponding hyperon in normal nuclear matter:

$$U_{\Lambda_c^+} = U_{\Lambda_b} = -30\mathrm{MeV},$$
$$U_{\Xi_c^0} = U_{\Xi_c^+} = -16\mathrm{MeV}. \tag{6}$$

Let's see the calculation results as the following. For lighter Lambda hypernuclei, the size of the core nucleus in a hypernucleus is smaller than the core nucleus in free space; i.e. the values of both $r_{\mathrm{n}}$ and $r_{\mathrm{p}}$ in a hypernucleus are less than those in the corresponding ordinary nucleus. For instance, the rms radius $r_{\mathrm{n}}$ ($r_{\mathrm{p}}$) of neutrons (protons) decreases from 2.32fm (2.37fm) in $^6$Li to 2.25fm (2.29fm) in $^7_\Lambda$Li. The attracting role of Lamda is obtained in agreement with the KEK-PS E419 experiment. But the situation for $\Xi$ hypernuclei is different. It is particularly of interest to observe a quite different effect caused by $\Xi$ hyperon impurities. The rms radii of the neutrons become a little larger, while the rms radii of the protons become much smaller, comparing with those in the normal nuclei. Contrary to the $\Xi^-$ hypernuclei, the rms radii of the protons become larger and those of the neutrons become smaller in the $\Xi^0$ hypernuclei.

What can we observe from the calculation results about the effect of different baryon impurities in nucleus? From all these results, we can draw the following conclusions:

First of all, systematic calculations show that $\Lambda_c^+$ and $\Lambda_b$ have the same attracting role as the $\Lambda$ hyperon does in lighter hypernuclei.

Next, the $\Xi^-$ and $\Xi_c^0$ hyperons have the attracting role only for the proton distribution and have a repulsive role for the neutron distribution.

On the contrary, $\Xi^0$ and $\Xi_c^+$ hyperons attract the surrounding neutrons and reveal a repulsive force to the protons.

Finally, we find that the different effects of different baryon impurities on the nuclear core are due to the different third components of their isospin.

## 3   Heavy flavored baryon hypernuclei[3]

Here heavy flavored baryon hypernuclei means charmed nuclei and bottom nuclei.

They will provide us with the first opportunity to learn about the behavior of heavy flavored hadrons in nuclear many-body systems.

Given the shortage of experimental data, can we theoretically estimate their Bound States? Let's use the relativistic mean-field model as theoretical framework. From Ref. [11], we can use the following coupling constants to the vector fields for the heavy flavored baryons,

$$g_{\omega\Lambda_c^+} = g_{\omega\Lambda_b} = \frac{2}{3}g_{\omega\mathrm{N}}, \quad g_{\omega\Xi_c^+} = g_{\omega\Xi_c^0} = \frac{1}{3}g_{\omega\mathrm{N}},$$
$$g_{\rho\Xi_c^+} = g_{\rho\Xi_c^0} = g_{\rho\mathrm{N}}. \tag{7}$$

And the coupling constants to the scalar field depend on the scalar field. They are fixed by the optical potential in our work.

$$U_{\mathrm{Y}} = g_{\sigma\mathrm{Y}}\sigma^{\mathrm{eq}} + g_{\omega\mathrm{Y}}\omega_0^{\mathrm{eq}} . \tag{8}$$

Thus, we investigated a number of theoretical values for the heavy flavored baryon potential well $U_{\mathrm{Y}}$. Here is an example by the theoretical estimates. Figure 3 shows the level space for $\Lambda_{\mathrm{b}}$ single-particle energies in $^{41}_{\Lambda_{\mathrm{b}}}$Ca and $^{208}_{\Lambda_{\mathrm{b}}}$Pb.
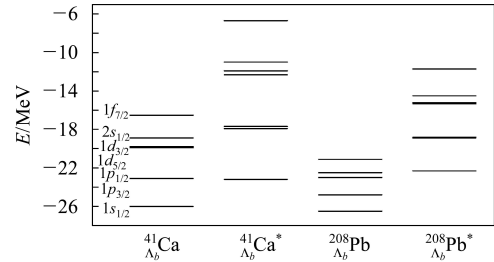


Fig. 3.   Level space for $\Lambda_{\mathrm{b}}$ single-particle energies in $^{41}_{\Lambda_{\mathrm{b}}}$Ca and $^{208}_{\Lambda_{\mathrm{b}}}$Pb.

In conclusion, we found that no $\Lambda_c^+$ or $\Xi_c^+$ bound states could exist if the potential well depths are in these ranges

$$\left|U_{\Lambda_c^+}\right| \leqslant 10\mathrm{MeV} \quad \text{or} \quad \left|U_{\Xi_c^+}\right| \leqslant 14\mathrm{MeV}, \tag{9}$$

in nuclear matter.

$$\text{If} \quad \left|U_{\Lambda_c^+}\right| \leqslant 20\mathrm{MeV} \quad \text{or} \quad \left|U_{\Xi_c^+}\right| \leqslant 18\mathrm{MeV},$$
$$\Lambda_c^+ \quad \text{or} \quad \Xi_c^+, \tag{10}$$

the $\Lambda_c^+$ and $\Xi_c^+$ hypernuclei cannot bind to the very heavy nuclei, for example $^{208}$Pb. We suggest that heavy systems be considered in the experimental searches for $\Lambda_c^+$ and $\Xi_c^+$ hypernuclei.

# 4　Eta-mesons in nuclear matter[4]

We have deduced the eta-nucleon interactions from the heavy-baryon chiral perturbation theory to the next-to-leading-order terms.

Combining the relativistic mean-field theory for nucleon system, we have studied the in-medium properties of the eta meson. We find that all the elastic-scattering ηN interactions come from the next-to-leading-order terms. And we found the eta-nucleon sigma term is about $280\pm130$MeV. The off-shell terms are also important to the in-medium properties of the eta meson.

On application of the latest determination of the eta-nucleon scattering length, the ratio of the eta-meson effective mass to its vacuum value is near $0.84\pm0.015$, whereas the optical potential is about $-(83\pm5)$MeV at the normal nuclear density.

The interactions between pseudoscalar mesons (pion, kaon, and eta mesons) and baryons (nucleons and hyperons) are described by the $SU(3)_{\mathrm{L}}\times SU(3)_{\mathrm{R}}$ chiral Lagrangian, which can be written as

$$\mathscr{L}_{\mathrm{chiral}} = \mathscr{L}_{\phi} + \mathscr{L}_{\phi\mathrm{B}} . \tag{11}$$

the mesonic term is

$$\mathscr{L}_{\phi} = \frac{1}{4}f^2\mathrm{Tr}\,\partial^{\mu}\Sigma\,\partial_{\mu}\Sigma^{\dagger} + \frac{1}{2}f^2 B_0[\mathrm{Tr}M_q(\Sigma-1)+\mathrm{h.c.}]. \tag{12}$$

the lowest order of meson-baryon interactions is

$$\mathscr{L}_{\phi\mathrm{B}}^{(1)} = \mathrm{Tr}\bar{B}(\mathrm{i}\gamma^{\mu}\partial_{\mu}-m_B)B + \mathrm{i}\mathrm{Tr}\bar{B}\gamma^{\mu}[V_{\mu},B] + D\mathrm{Tr}\bar{B}\gamma^{\mu}\gamma^5\{A_{\mu},B\} + F\mathrm{Tr}\bar{B}\gamma^{\mu}\gamma^5[A_{\mu},B], \tag{13}$$

the next-to-leading order of meson-baryon interactions is

$$\begin{aligned}
\mathscr{L}_{\phi\mathrm{B}}^{(2)} = {}& a_1\mathrm{Tr}\bar{B}(\xi M_q\xi+\mathrm{h.c.})B + \\
& a_2\mathrm{Tr}\bar{B}B(\xi M_q\xi+\mathrm{h.c.}) + \\
& a_3\mathrm{Tr}\bar{B}B\mathrm{Tr}(M_q\Sigma+\mathrm{h.c.}) + \\
& d_1\mathrm{Tr}\bar{B}A^2B + d_2\mathrm{Tr}\bar{B}(vA)^2B + \\
& d_3\mathrm{Tr}\bar{B}BA^2 + d_4\mathrm{Tr}\bar{B}B(vA)^2 + \\
& d_5\mathrm{Tr}\bar{B}B\mathrm{Tr}A^2 + d_6\mathrm{Tr}\bar{B}B\mathrm{Tr}(vA)^2 + \\
& d_7\mathrm{Tr}\bar{B}A_{\mu}\mathrm{Tr}A^{\mu}B + d_8\mathrm{Tr}\bar{B}(vA)\mathrm{Tr}(vA)B + \\
& d_9\mathrm{Tr}\bar{B}A_{\mu}BA^{\mu} + d_{10}\mathrm{Tr}\bar{B}(vA)B(vA). \tag{14}
\end{aligned}$$

The calculated results are listed in Table 1 of Ref. [4]. Recent eta-N scattering length in literature is about 0.717—1.14fm. Thus, the potential depth is about 63—88MeV in our predictions.

# 5　The properties of kaonic nuclei[5]

In K-nucleus, a Kaon does not suffer from Pauli blocking, it can locate at the center of a nucleus; then, the Kaon attracts surrounding nucleons and makes the nucleus shrink.

We have studied these properties of kaonic nuclei from C to Ti in the relativistic mean-field theory. The $1s$ and $1p$ state binding energies of Kaon are in the range of 73—96MeV and 22—63MeV, respectively. The binding energies of $1p$ states increase monotonically with the nucleon number A. We also calculated the upper limit and the lower limit of the widths for the $1s$ states and the $1p$ states. We show that if $V_0$ is less than or equals to 30MeV, the discrete Kaon bound states should be identified in experiment. We find that the interior nuclear density increases obviously, and the densest center density is about 2.1 times the normal nuclear density.

We now show the equations of motion for describing the K-nucleus system. For nucleon system the equations of motion are:

$$\begin{aligned}
& [-\mathrm{i}\boldsymbol{\alpha}\cdot\boldsymbol{\nabla}+\beta(M_{\mathrm{N}}+g_{\sigma\mathrm{N}}\sigma_0)+g_{\omega\mathrm{N}}\omega_0+ \\
& g_{\rho\mathrm{N}}\tau_3\rho_0+eI_{\mathrm{c}}A_0]\Psi_{\mathrm{N}} = \epsilon\Psi_{\mathrm{N}},
\end{aligned}$$

$$\begin{aligned}
(-\nabla^2+m_{\sigma}^2)\sigma_0 = {}& -g_{\sigma\mathrm{N}}\bar{\Psi}_{\mathrm{N}}\Psi_{\mathrm{N}}-g_2\sigma_0^2-g_3\sigma_0^3- \\
& g_{\sigma\mathrm{K}}m_{\mathrm{K}}\bar{K}K,
\end{aligned}$$

$$\begin{aligned}
(-\nabla^2+m_{\omega}^2)\omega_0 = {}& -g_{\omega\mathrm{N}}\bar{\Psi}_{\mathrm{N}}\gamma^0\Psi_{\mathrm{N}}- \\
& 2g_{\omega\mathrm{K}}(E+g_{\omega\mathrm{K}}\omega_0)\bar{K}K,
\end{aligned}$$

$$(-\nabla^2+m_{\rho}^2)\rho_0 = g_{\rho\mathrm{N}}\bar{\Psi}_{\mathrm{N}}\gamma^0 I\Psi_{\mathrm{N}},$$

$$-\nabla^2 A_0 = e\Psi_{\mathrm{N}}\gamma^0 I_{\mathrm{c}}\Psi_{\mathrm{N}}, \tag{15}$$

and the equation of motion for antikaon is

$$[-\nabla^2+(m_{\mathrm{K}}^2-E^2)+\Pi]\bar{K} = 0, \tag{16}$$

with the antikaon self-energy in nuclei

$$\Pi = -2g_{\omega\mathrm{K}}E\omega_0+g_{\sigma\mathrm{K}}m_{\mathrm{K}}\sigma_0-(g_{\omega\mathrm{K}}\omega_0)^2 . \tag{17}$$

shown with the antikaon self-energy in nuclei calculated.

Table 1.   The r.m.s. radii of neutron, proton and charge distribution, respectively.

|  | $V_0$ | $r_{\rm p}$ | $r_{\rm n}$ | $r_{\rm ch}$ |  | $V_0$ | $r_{\rm p}$ | $r_{\rm n}$ | $r_{\rm ch}$ |  | $-V_0$ | $r_{\rm p}$ | $r_{\rm n}$ | $r_{\rm ch}$ |
|---|---|---|---|---|---|---|---|---|---|---|---|---|---|---|
| $^{12}$C |  | 2.32 | 2.30 | 2.46 | $^{24}$Mg |  | 2.86 | 2.82 | 2.97 | $^{36}$Ar |  | 3.26 | 3.21 | 3.36 |
| $^{12}$CK$^-$ | 15 | 2.20 | 2.18 | 2.35 | $^{24}$MgK$^-$ | 15 | 2.80 | 2.77 | 2.92 | $^{36}$ArK$^-$ | 15 | 3.22 | 3.17 | 3.32 |
|  | 30 | 2.20 | 2.18 | 2.35 |  | 30 | 2.80 | 2.77 | 2.92 |  | 30 | 3.22 | 3.17 | 3.32 |
|  | 50 | 2.21 | 2.19 | 2.35 |  | 50 | 2.80 | 2.77 | 2.92 |  | 50 | 3.22 | 3.18 | 3.33 |
| $^{16}$O |  | 2.58 | 2.55 | 2.70 | $^{28}$Si |  | 2.93 | 2.90 | 3.04 | $^{40}$Ca |  | 3.36 | 3.31 | 3.46 |
| $^{16}$OK$^-$ | 15 | 2.52 | 2.49 | 2.65 | $^{28}$SiK$^-$ | 15 | 2.88 | 2.85 | 2.99 | $^{40}$CaK$^-$ | 15 | 3.32 | 3.27 | 3.42 |
|  | 30 | 2.51 | 2.49 | 2.64 |  | 30 | 2.88 | 2.85 | 2.99 |  | 30 | 3.32 | 3.28 | 3.42 |
|  | 50 | 2.51 | 2.48 | 2.64 |  | 50 | 2.88 | 2.85 | 2.99 |  | 50 | 3.32 | 3.28 | 3.43 |
| $^{20}$Ne |  | 2.82 | 2.74 | 2.94 | $^{32}$S |  | 3.13 | 3.09 | 3.24 | $^{44}$Ti |  | 3.44 | 3.39 | 3.54 |
| $^{20}$NeK$^-$ | 15 | 2.77 | 2.69 | 2.89 | $^{32}$SK$^-$ | 15 | 3.08 | 3.04 | 3.19 | $^{44}$TiK$^-$ | 15 | 3.41 | 3.36 | 3.50 |
|  | 30 | 2.77 | 2.68 | 2.89 |  | 30 | 3.08 | 3.04 | 3.19 |  | 30 | 3.41 | 3.36 | 3.50 |
|  | 50 | 2.76 | 2.68 | 2.88 |  | 50 | 3.09 | 3.04 | 3.20 |  | 50 | 3.41 | 3.36 | 3.51 |

To include the antikaon absorptions in a nucleus, we introduce a complex potential in the realistic calculations.

$$\tilde{\Pi} = \big[-2g_{\omega{\rm K}}\omega_0{\rm Re}E + g_{\sigma{\rm K}}m_{\rm K}\sigma_0 - (g_{\omega{\rm K}}\omega_0)^2\big] +$$

$$i\left[-2({\rm Re}E)fV_0\frac{\rho}{\rho_0}\right]. \tag{18}$$

The imaginary part is given with the simple "$t$-rho" form. "$f$" is a suppression factor for the phase space available. The decay products should be reduced for deeply bound states, which will decrease the imaginary potentials. The details of the binding energies of K nucleus system are in Ref. [5]. Table 1 shows the r.m.s. radii of neutron, proton and charge distribution, respectively.

The shrinkage is also predicted in kaonic nuclei. Fig. 4 shows the nucleon-density as a function of nucleus radius. The solid and dotted curves are for the kaonic nuclei and the corresponding ordinary nuclei,

respectively. We can see that the interior nuclear densities become denser than those of the ordinary nuclei. But, the interior nuclear densities do not increase drastically. The densest nuclear density is about 2.1 times the normal nuclear density.
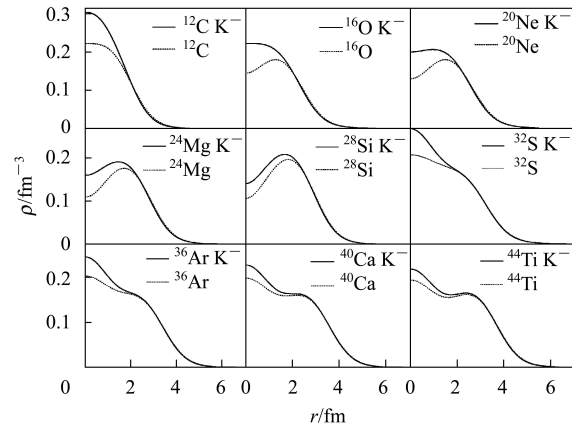


Fig. 4.   Nucleon-density as a function of nucleus radius for kaonic nuclei.

## References

1　WANG Q L et al. Europhys. Lett., 2006, **75**(1): 36—41

2　TAN Yu-Hong et al. Phys. Rev., 2004, **C70**: 054306

3　TAN Yu-Hong, NING Ping-Zhi. Europhys. Lett., 2004, **67**(3): 355—361

4　ZHONG X H et al. Phys. Rev., 2006, **C73**: 015205

5　ZHONG X H et al. Phys. Rev., 2006, **C74**: 034321

6　ZHONG X H et al. Phys. Rev., 2005, **C71**: 015206

7　ZHONG X H, PENG G X, NING P Z. Phys. Rev., 2005, **C72**: 065212

8　YAO Jiang-Ming et al. HEP & NP, 2005, **29**: 105 (in Chinese)

（尧江明等. 高能物理与核物理, 2005, **29**: 105）

9　ZHONG Xian-Hui et al. Commun. Theor. Phys., 2004, **41**: 573—578

10　TAN Yu-Hong, NING Ping-Zhi. Eur. Phys. J., 2004, **A20**: 257—262

11　Cooper et al. Nucl. Phys., 1994, **A580**: 419; 1995, **585**: 157c

# 南开大学奇异性核物理的理论研究

## 宁平治

(南开大学物理科学学院　天津　300071)

**摘要**　简要介绍了南开大学核物理组在奇异性核物理方面的理论研究工作. 已经完成的工作有核介质内超子平均自由程的理论计算, 奇异性核物理方面已完成的其他4个理论研究课题是, 不同重子杂质对原子核的影响、重味重子超核、核物质内的eta-介子以及K介子原子核的性质.

**关键词**　核物理　奇异性　超子